An Introduction to Earthquake Location

Qi Yingyu

Nanyang Technological University

Outline

Geiger's Method

Assumption

Let the coordinates of the earthquake be (x, y, z, T), where x, y and z are the spatial coordinates and T is the origin time.
Reference: 1. Geiger, L. (1912). Probability method for the determination of earthquake epicenters from the arrival time only. Bull. St. Louis Univ, 8(1), 56-71.
program: HYPOLAYR, HYPO71, HYPO78-86, HYPOELLIPSE,HYPOINVERSE,QUAKE3D.
$https://pubs.usgs.gov/of/1999/ofr-99-0023/$

$$res = t_{observed} - t_{predicted}$$

$$t_{predicted} = T + \frac{1}{c}\sqrt{(x-x_0)^2 + (y-y_0)^2 + (z-z_0)^2}$$

$$-res = \frac{\partial t}{\partial x}\Delta x + \frac{\partial t}{\partial y}\Delta y + \frac{\partial t}{\partial z}\Delta z + \Delta T.$$

Joint Epicentre Determination

$$\Delta t = \Delta T + \Delta h \frac{\partial T}{\partial h} + x \cos\alpha \frac{\partial T}{\partial E} - y \sin\alpha \frac{\partial T}{\partial E}$$

$$\Delta t = \Delta T + \Delta h \frac{\partial T}{\partial h} + x \cos\alpha \frac{\partial T}{\partial E} - y \sin\alpha \frac{\partial T}{\partial E} + \Delta S$$

Assumption

$x, y, \Delta h, \Delta T$ are the corrections to latitude, longitude, depth and origin time, respectively. α is the azimuth to station. S is the difference between the observed travel time and the travel time obtained from the travel time tables(taup). $\sum S = 0$. E is the epicenter distance.

Reference : Douglas, A. (1967). Joint epicentre determination. Nature, 215(5096), 47-48.

Joint Epicentre Determination

ak135

P

Δ	Depth of source [km] 0.	15.	35.	50.	100.	150.	200.	250.
	m s	m s	m s	m s	m s	m s	m s	m s
0.0	0 00.00	0 02.59	0 05.76	0 07.62	0 13.84	0 20.03	0 26.12	0 32.11
	19.17	*0.01*	*0.00*	*0.00*	*0.00*	*0.00*	*0.00*	*0.00*
1.0	0 19.17	0 19.01	0 17.51	0 17.70	0 20.39	0 24.73	0 29.72	0 34.99
	19.17	*17.05*	*13.75*	*13.45*	*10.82*	*8.46*	*6.74*	*5.51*
2.0	0 35.03	0 33.23	0 31.27	0 31.32	0 32.54	0 35.08	0 38.47	0 42.42
	13.75	*13.75*	*13.75*	*13.69*	*12.90*	*11.63*	*10.27*	*9.01*
3.0	0 48.78	0 46.98	0 45.02	0 45.02	0 45.71	0 47.32	0 49.59	0 52.43
	13.75	*13.75*	*13.75*	*13.71*	*13.35*	*12.66*	*11.77*	*10.81*
4.0	1 02.53	1 00.73	0 58.77	0 58.74	0 59.14	1 00.20	1 01.73	1 03.75
	13.75	*13.75*	*13.75*	*13.72*	*13.49*	*13.06*	*12.44*	*11.72*
5.0	1 16.27	1 14.47	1 12.51	1 12.45	1 12.67	1 13.36	1 14.35	1 15.74
	13.74	*13.74*	*13.74*	*13.72*	*13.55*	*13.24*	*12.76*	*12.20*
6.0	1 30.01	1 28.21	1 26.25	1 26.17	1 26.24	1 26.64	1 27.20	1 28.08
	13.74	*13.74*	*13.73*	*13.71*	*13.58*	*13.32*	*12.92*	*12.46*
7.0	1 43.75	1 41.94	1 39.98	1 39.88	1 39.83	1 39.98	1 40.17	1 40.62
	13.73	*13.73*	*13.73*	*13.71*	*13.60*	*13.35*	*13.00*	*12.59*
8.0	1 57.47	1 55.67	1 53.70	1 53.58	1 53.42	1 53.33	1 53.18	1 53.24
	13.72	*13.72*	*13.72*	*13.70*	*13.60*	*13.34*	*13.02*	*12.65*
9.0	2 11.19	2 09.38	2 07.41	2 07.27	2 07.02	2 06.66	2 06.20	2 05.89
	13.71	*13.71*	*13.71*	*13.69*	*13.60*	*13.30*	*13.00*	*12.64*
10.0	2 24.90	2 23.09	2 21.12	2 20.96	2 20.62	2 19.93	2 19.17	2 18.51
	13.70	*13.70*	*13.70*	*13.68*	*13.59*	*13.24*	*12.93*	*12.59*
11.0	2 38.59	2 36.78	2 34.81	2 34.63	2 34.21	2 33.12	2 32.05	2 31.06
	13.69	*13.69*	*13.68*	*13.66*	*13.59*	*13.14*	*12.82*	*12.51*
12.0	2 52.27	2 50.46	2 48.48	2 48.29	2 47.59	2 46.19	2 44.80	2 43.51
	13.67	*13.67*	*13.67*	*13.65*	*13.28*	*13.00*	*12.68*	*12.40*
13.0	3 05.94	3 04.13	3 02.14	3 01.93	3 00.80	2 59.10	2 57.41	2 55.85
	13.66	*13.66*	*13.65*	*13.64*	*13.13*	*12.82*	*12.52*	*12.27*
14.0	3 19.59	3 17.78	3 15.79	3 15.56	3 13.83	3 11.81	3 09.85	3 08.06
	13.64	*13.64*	*13.64*	*13.62*	*12.93*	*12.61*	*12.36*	*12.13*
15.0	3 33.23	3 31.41	3 29.32	3 28.75	3 26.63	3 24.32	3 22.13	3 19.74
	13.63	*13.19*	*13.14*	*13.03*	*12.66*	*12.41*	*12.20*	*11.02*
16.0	3 46.37	3 44.46	3 42.31	3 41.62	3 39.17	3 36.64	3 33.83	3 30.73
	12.94	*12.90*	*12.82*	*12.70*	*12.43*	*12.22*	*11.01*	*10.97*
17.0	3 59.13	3 57.17	3 54.96	3 54.17	3 51.49	3 48.19	3 44.81	3 41.67
	12.58	*12.55*	*12.50*	*12.42*	*12.22*	*11.00*	*10.95*	*10.89*

Joint Epicentre Determination

Table 2

Station	Azimuth	Station correction	LONGSHOT residual Observed − J−B time
MBC	23·0	−0·7	Not available
COL	41·0	−1·5	−3·6
WES	51·8	−0·9	−5·1
OTT	52·3	−1·8	−5·9
SJG	62·8	−1·0	−4·2
CPO	66·0	−1·9	−5·0
BMO	77·9	+0·0	−2·7
UBO	78·1	+0·5	−1·7
PAS	90·9	−0·3	−2·4
KIP	148·1	+2·9	−0·6
PPT	152·8	+1·9	−1·9
VUN	184·5	+2·4	−2·0
KOU	198·0	+0·8	−1·8
HNR	205·0	+1·2	−2·5
RIV	206·0	+2·2	−1·9
BRS	206·6	+0·0	−2·5
TOO	209·1	+2·0	−2·6
CTA	214·8	−1·1	−3·5
PMG	217·9	−0·4	−2·9
DAR	231·7	−0·1	−2·9
MAT	259·4	−0·0	−2·5
SHL	286·6	−1·4	−3·6
QUE	307·8	−0·1	−2·5
TEH	322·0	+0·4	−3·1
IST	340·4	−0·5	−5·4
UPP	352·0	−1·1	−5·1
TRO	353·4	−0·1	−4·0
CLL	353·5	−0·6	Not available
STU	355·7	−0·4	Not available
KON	356·3	−0·7	−4·2

Joint Epicentre Determination

Table 1

(1) Komandorsky Isles: July 19, 1966			
USCGS epicentre	56·20 N. 164·90 E.	$h = 18$ km	$H = 1 : 40 : 53·9$
Epicentre using thirty stations	56·43 N. 164·46 E.	$h = 18$ km*	$H = 1 : 40 : 54·9$
Epicentre using joint method	56·28 N. 164·62 E.	$h = 18$ km*	$H = 1 : 40 : 54·8$
(2) Rat Islands, Aleutian Islands: June 2, 1966			
USCGS epicentre	51·08 N. 175·97 E.	$h = 41$ km*	$H = 3 : 27 : 53·3$
Epicentre using thirty stations	51·04 N. 175·89 E.	$h = 41$ km*	$H = 3 : 27 : 52·9$
Epicentre using joint method	50·92 N. 175·98 E.	$h = 41$ km*	$H = 3 : 27 : 53·2$
(3) Rat Islands, Aleutian Islands (LONGSHOT): October 29, 1965			
True epicentre	51·44 N. 179·18 E.	$h = 0$ km*	$H = 21 : 0 : 0·1$
Epicentre using thirty stations	51·65 N. 179·13 E.	$h = 0$ km*	$H = 20 : 59 : 56·9$
Epicentre using joint method	51·45 N. 179·18 E.	$h = 0$ km*	$H = 20 : 59 : 56·8$
(4) Andreanof Islands, Aleutian Islands: July 19, 1966			
USCGS epicentre	51·73 N. 173·30 W.	$h = 47$ km*	$H = 19 : 20 : 33·4$
Epicentre using thirty stations	51·81 N. 173·35 W.	$h = 47$ km*	$H = 19 : 20 : 33·5$
Epicentre using joint method	51·75 N. 173·40 W.	$h = 47$ km*	$H = 19 : 20 : 33·9$
(5) Fox Islands, Aleutian Islands: August, 11, 1966			
USCGS epicentre	52·76 N. 169·74 W.	$h = 61$ km	$H = 10 : 45 : 59·6$
Epicentre using thirty stations	52·76 N. 169·77 W.	$h = 61$ km*	$H = 10 : 45 : 59·1$
Epicentre using joint method	52·71 N. 169·79 W.	$h = 61$ km*	$H = 10 : 45 : 59·6$
(6) South of Alaska: February 6, 1965			
USCGS epicentre	53·29 N. 161·81 W.	$h = 33$ km*	$H = 16 : 50 : 28·6$
Epicentre using thirty stations	53·24 N. 161·88 W.	$h = 33$ km*	$H = 16 : 50 : 28·2$
Epicentre using joint method	53·06 N. 161·92 W.	$h = 33$ km*	$H = 16 : 50 : 28·2$
(7) South of Alaska: January 22, 1966			
USCGS epicentre	55·97 N. 153·69 W.	$h = 33·0$ km*	$H = 14 : 27 : 7·9$
Epicentre using thirty stations	55·96 N. 153·89 W.	$h = 33·0$ km*	$H = 14 : 27 : 7·8$
Epicentre using joint method	55·83 N. 153·93 W.	$h = 33·0$ km*	$H = 14 : 27 : 7·7$

* Restrained parameters.

Joint Hypocenter Determination

$$w_{ij} r_{ij} = w_{ij}\left(dT_j + \frac{\partial t}{\partial x_j} dx_j + \frac{\partial t}{\partial y_j} dy_j + \frac{\partial t}{\partial z_j} dz_j + ds_i \right);$$

$$i=1,N;\ j=1,M$$

where

$$r_{ij} = t_{ij}^{o} - (T_j + \tau_{ij} + s_i)$$

JED and JHD

The only difference between single-event location and JHD is the occurrence in the latter of a correction term for each of the *N* stations.

Reference : Pujol, J. (2000). Joint event locationthe JHD technique and applications to data from local seismic networks. In Advances in seismic event location (pp. 163-204). Springer, Dordrecht.

JHD

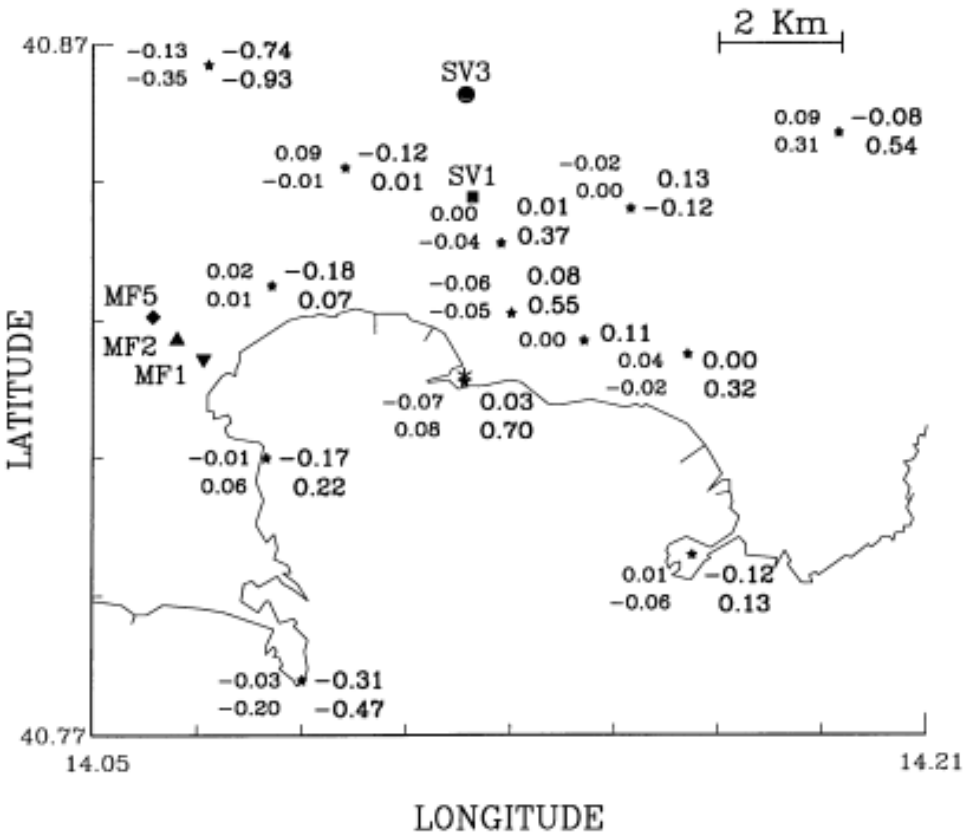

Figure 14. Stations used to locate the Campi Flegrei events (stars). The upper and lower numbers on the right of the stations are P- and S-wave JHD† station corrections (in seconds), respectively. The numbers on the left are the corresponding average residuals (Equation 34). One station does not have S-wave information. Note the large magnitude of some of the corrections and the much smaller magnitude of the corresponding residuals. The dot, square, diamond and triangles represent boreholes with P-wave sonic velocities available in the San Vito (SV) and Mofete (MF) areas. Modified from Pujol (2000).

JHD

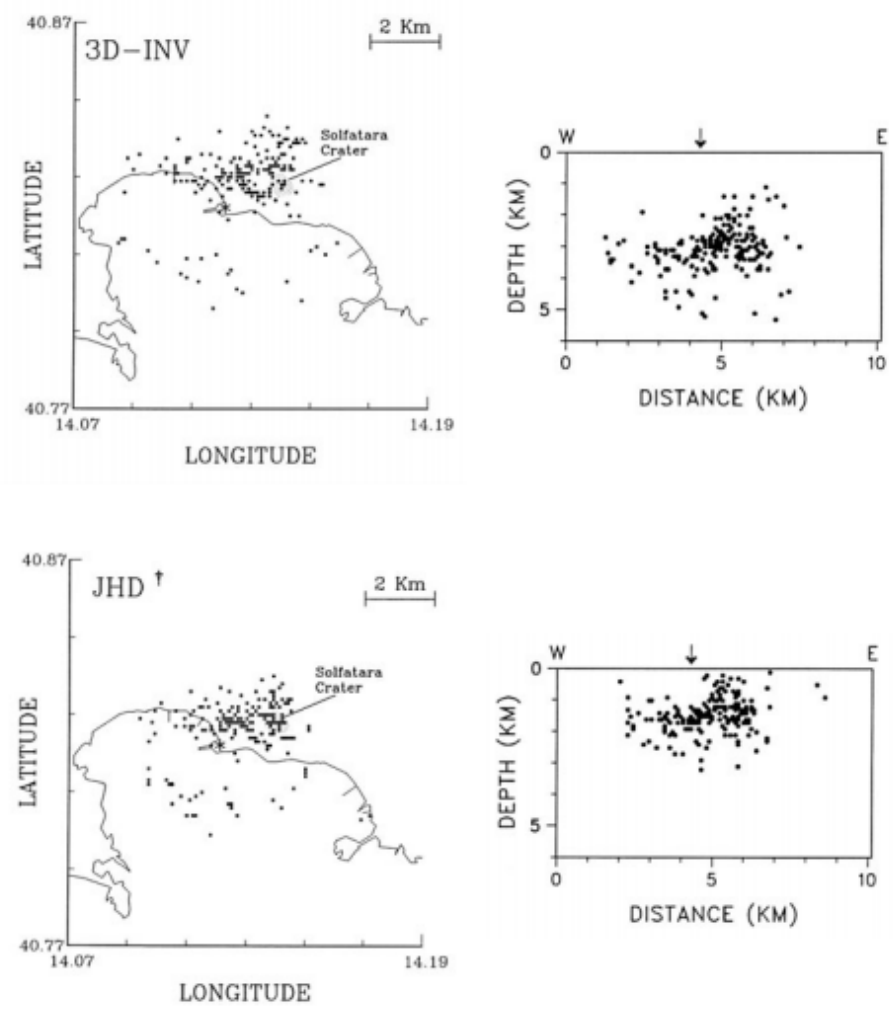

Figure 13. Epicenters of Campi Flegrei events (left) and W-E cross sections (right). Locations from Pujol and Aster (1990). The asterisk near the center of the epicentral map represents the town of Pozzuoli (shown by an arrow in the cross sections). The Solfatara crater was the only volcanic feature active during the uplift episode. Modified from Pujol (2000).

Frohlich Simplification (1979)

Process

1. Locate each earthquake individually.
2. For the i-th station average the residuals for all the events.
3. Relocate the events using the average residuals as station corrections.
4. Optionally, iterate steps $1 - 3$.

Reference : Frohlich, C. (1979). An efficient method for joint hypocenter determination for large groups of earthquakes. Computers & Geosciences, 5(3-4), 387-389.

$$ds_i \approx a_i = \frac{1}{\left(\sum_{j=1}^{M} w_{ij}^2\right)} \sum_{j=1}^{M} w_{ij}^2 \, r_{ij}$$

Frohlich Simplification (1979)

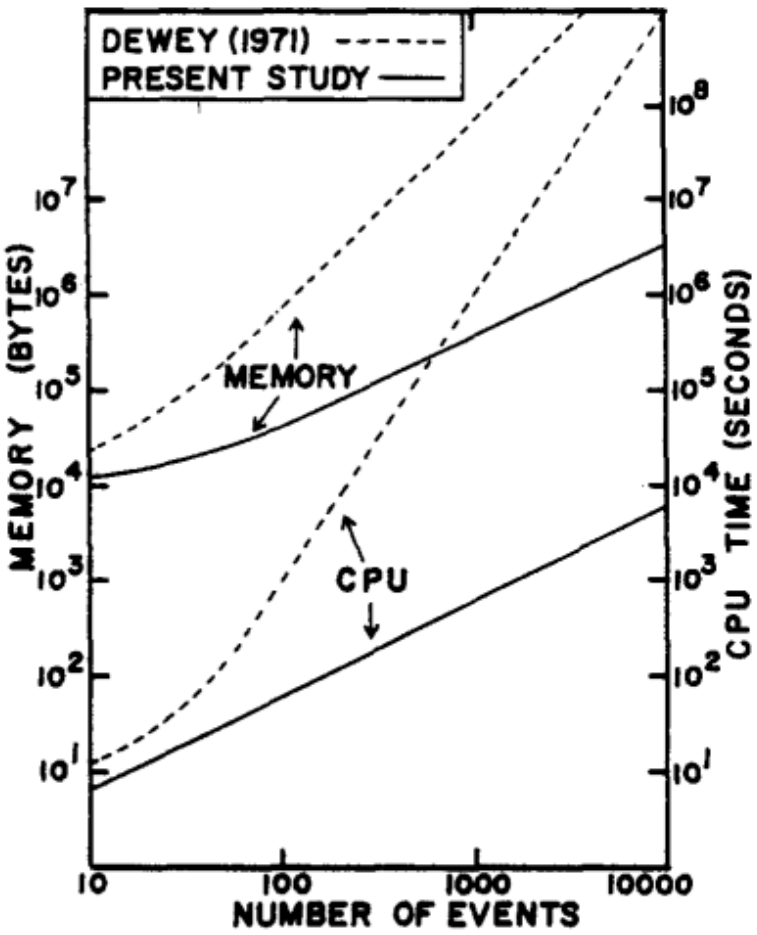

Figure 1. Comparison of computer memory and central processor unit (CPU) time necessary to perform four iterations of hypocentral improvement on IBM 370/168 at Cornell University using program of Dewey (1971) and program written for this study.

Joint Inversion

3D joint inversion

x and α refer to the hypocenter location and velocity model parameters respectively.

Reference : Crosson, R. S. (1976). Crustal structure modeling of earthquake data: 1. Simultaneous least squares estimation of hypocenter and velocity parameters. Journal of geophysical research, 81(17), 3036-3046.

$$\mathbf{T}_{ij} = \mathbf{T}_{ij}(\mathbf{x}_{1i}, \mathbf{x}_{2i}, \mathbf{x}_{3i}, \mathbf{x}_{4i}, \alpha_1, \cdots, \alpha_l) \qquad (1)$$

$$i = 1, \cdots, \mathbf{q} \qquad j = 1, \cdots, \mathbf{p}$$

$$\Delta\mathbf{T}_{ij} = \sum_{k=1}^{4} \left(\frac{\partial \mathbf{T}_{ij}}{\partial \mathbf{x}_{ki}}\right) \Delta\mathbf{x}_{ki} + \sum_{k=1}^{l} \left(\frac{\partial \mathbf{T}_{ij}}{\partial \alpha_k}\right) \Delta\alpha_k \qquad (2)$$

where

$$\Delta\mathbf{T}_{ij} = \mathbf{T}_{ij} - \mathbf{T}_{ij}^{0} \qquad \Delta\mathbf{x}_{ki} = \mathbf{x}_{ki} - \mathbf{x}_{ki}^{0} \qquad \Delta\alpha_k = \alpha_k - \alpha_k^{0}$$

SSH results

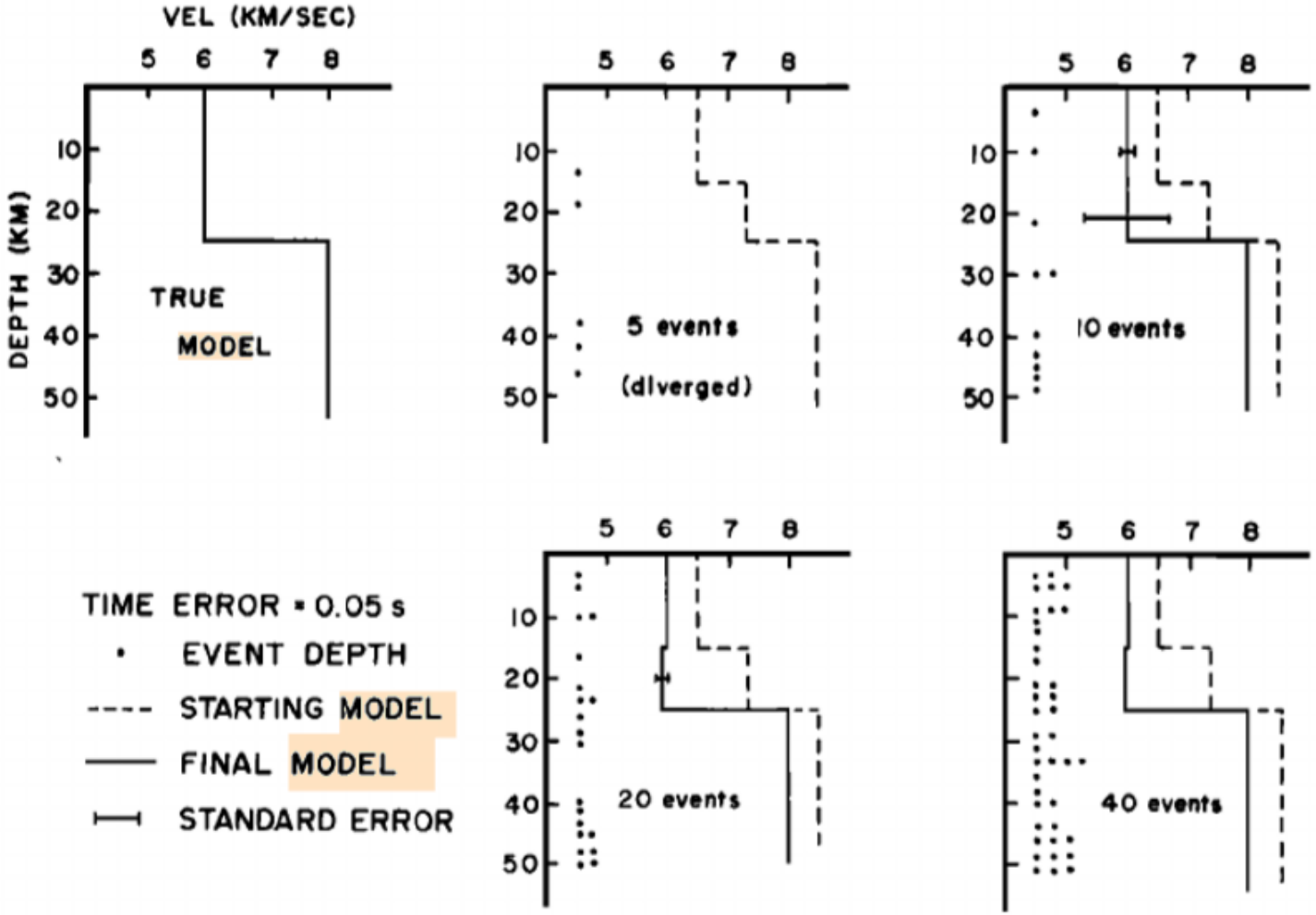

Fig. 4. Sequence of inversion runs illustrating the effect of increasing the number of events. Velocity error bounds are decreased as more data are added, with little improvement realized above 20 events. The upper two layer velocities for the inverted model converge correctly to the same value, since the true model has only two layers.

SSH results

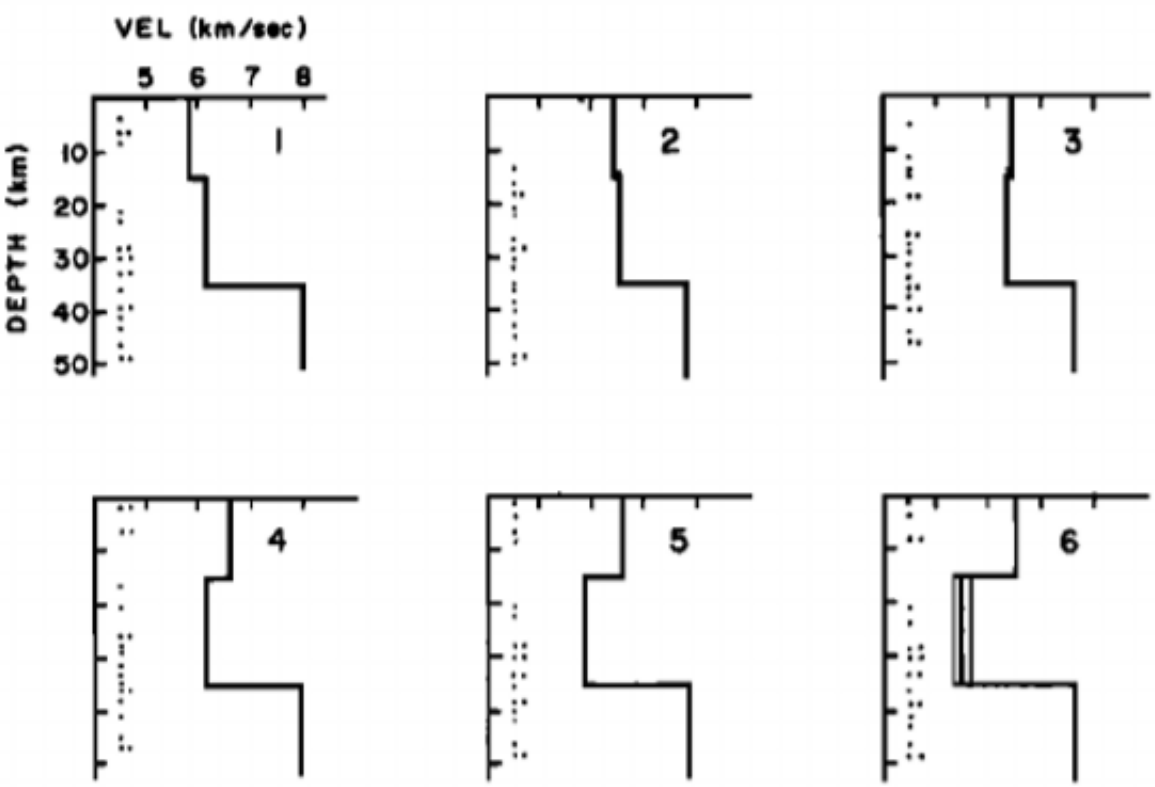

Fig. 5. History of convergence of classical least squares applied to a three-layer model with a low-velocity layer. Convergence is achieved in six iterations. Standard error bounds (light line) in frame 6 indicate that the LVL velocity is less well determined than the LVL velocity for adjacent layers. Error bounds for the top and bottom layers are within line width.

SSH results

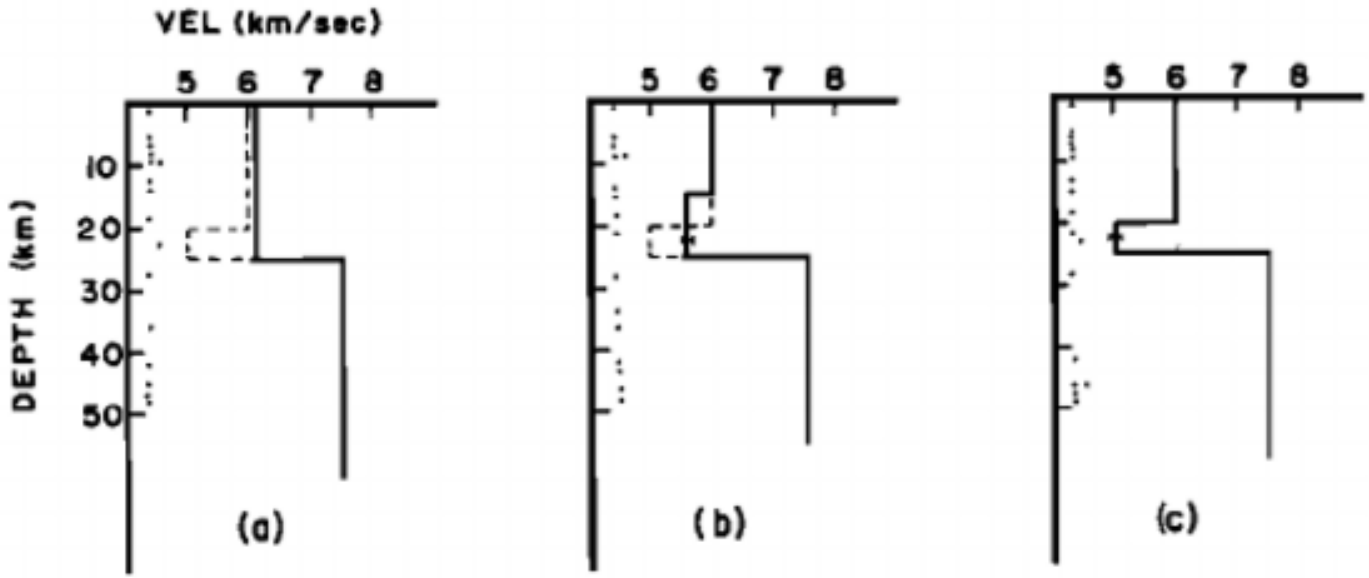

Fig. 6. Example showing three different parameterizations for the same set of data generated on a model with a thin low-velocity layer. (*a*) The LVL is ignored completely when the inverted model is two layer. (*b*) A middle layer of incorrect thickness estimates an average velocity over the interval. (*c*) With layer boundaries correct, the correct velocity is estimated. Error bars indicate standard errors where they are greater than line width. The true model is indicated by dashed lines, the inverted model by solid lines, and the hypocenter depth by dots.

Outline

The Arrival-Time Difference Method (ATD)

Assumption

$$A_{Qk} = f(H, \phi, \lambda, h)_Q$$

Earthquake Q, origin time H, latitude ϕ, longitude λ, focal depth h, seismic station k.

$$A_{Qk} = f(h, \phi, \lambda, h)_y + \left\{\frac{\partial A_k}{\partial H}\right\}_{\phi_y, \lambda_y, h_y} \delta H$$
$$+ \left\{\frac{\partial A_k}{\partial \phi}\right\}_{H_y, \lambda_y, h_y} \delta\phi + \left\{\frac{\partial A_k}{\partial \lambda}\right\}_{H_y, \phi_y, h_y} \delta\lambda$$
$$+ \left\{\frac{\partial A_k}{\partial h}\right\}_{H_y, \phi_y, \lambda_y} \delta h + \text{higher order terms}$$

The Arrival-Time Difference Method (ATD)

Assumption

$$A_{Qk} = f(H, \phi, \lambda, h)_Q$$

Earthquake Q, origin time H, latitude ϕ, longitude λ, focal depth h, seismic station k.

Reference : 1. Newcomb, S. (1906). A compendium of spherical astronomy with its applications to the determination and reduction of positions of the fixed stars. Macmillan.

2.Spence, W. (1980). Relative epicenter determination using P-wave arrival-time differences. Bulletin of the Seismological Society of America, 70(1), 171-183.

$$A_{Qk} = f(h, \phi, \lambda, h)_y + \left\{\frac{\partial A_k}{\partial H}\right\}_{\phi_y, \lambda_y, h_y} \delta H + \left\{\frac{\partial A_k}{\partial \phi}\right\}_{H_y, \lambda_y, h_y} \delta\phi + \left\{\frac{\partial A_k}{\partial \lambda}\right\}_{H_y, \phi_y, h_y} \delta\lambda + \left\{\frac{\partial A_k}{\partial h}\right\}_{H_y, \phi_y, \lambda_y} \delta h + \text{higher order terms}$$

ATD

$$\delta\tau_k = \delta H + \left(\frac{\partial A}{\partial \Delta}\cos G_k\right)S + \frac{\partial A}{\partial h}\,\delta h + \frac{1}{2!}\left(\frac{\partial A}{\partial \Delta}\cot\Delta\sin^2 G_k + \frac{\partial^2 A}{\partial \Delta^2}\cos^2 G_k\right)S^2$$

$$k = 1, N. \quad (11)$$

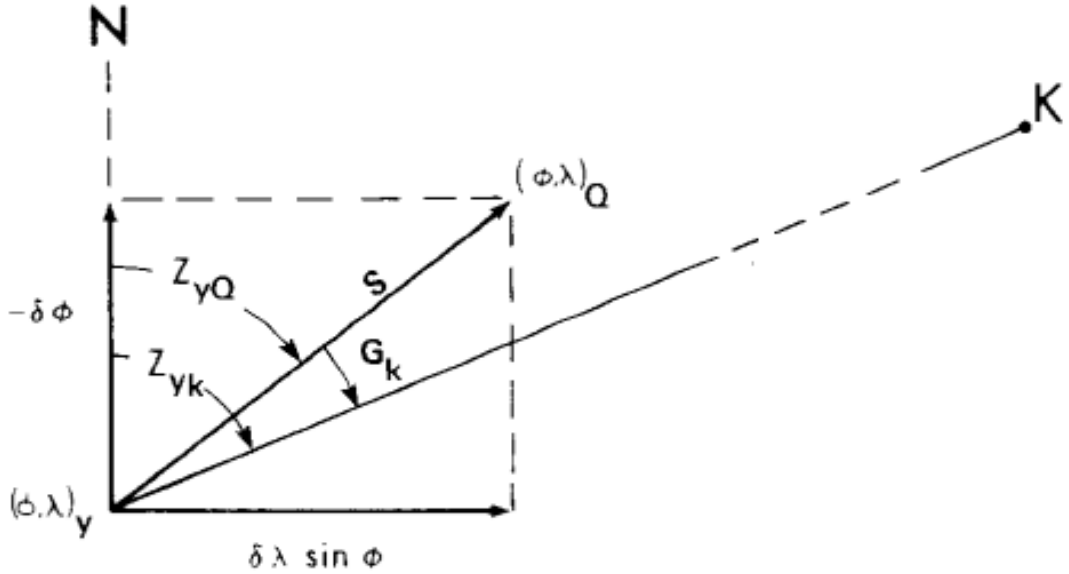

FIG. 1. Geometry for the rotation of axes, which results in $\delta\phi \to S$ and $\delta\lambda \to 0$ in equation (9). Diagram also applies to equations (1) and (13), where R substitutes for y, x for Q, and Z_{Rk} for G_k.

ATD

$$\delta t_k = (A_{xk} - A_{Rk}) = \delta H + \frac{\partial A}{\partial \Delta} \cos Z_{Rk} \delta\phi - \frac{\partial A}{\partial \Delta} \sin \phi_R \sin Z_{Rk} \delta\lambda + \frac{\partial A}{\partial h} \delta h; \quad k = 1, N, \quad (13)$$

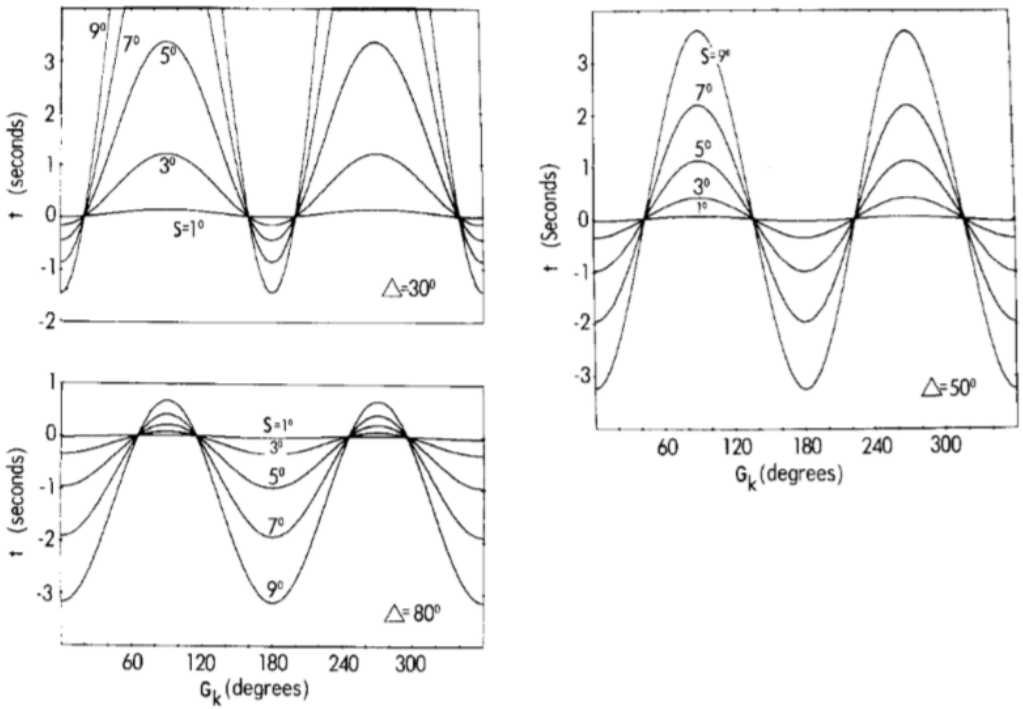

FIG. 3. Graphs of the Jeffreys-Bullen (1940) time values for the second-order terms in equation (11), as a function of azimuth G_k, for $S = 1°, 3°, 5°, 7°$, and $9°$. The geometric second-order terms dominate for $\Delta = 30°$, the $\partial^2/\partial\Delta^2$ terms are large for $\Delta = 80°$ and very large for $\Delta \leqq 25°$, and these two components of the second-order terms are about equal for $\Delta = 50°$.

ATD Results

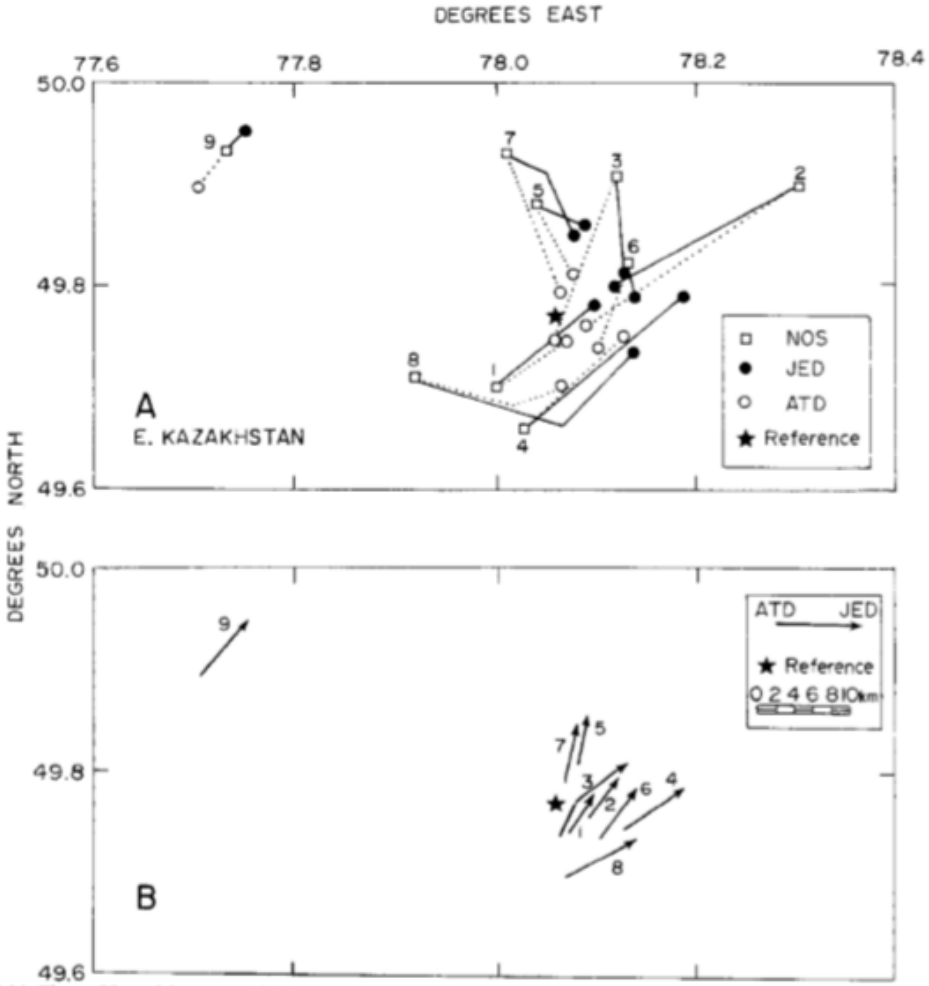

FIG. 4. (A) East Kazakhstan, USSR, nuclear shot relocations using both the ATD and JED models (star shows position of reference event for ATD relocations and position of constrained event for JED relocations). Relocations are shown with respect to the standard single-event locations as determined by the National Ocean Survey (NOS). (B) ATD-JED location difference vectors. While the relocation patterns determined with the ATD and JED models are very similar, there is a systematic location difference shown by these vectors.

ATD Results

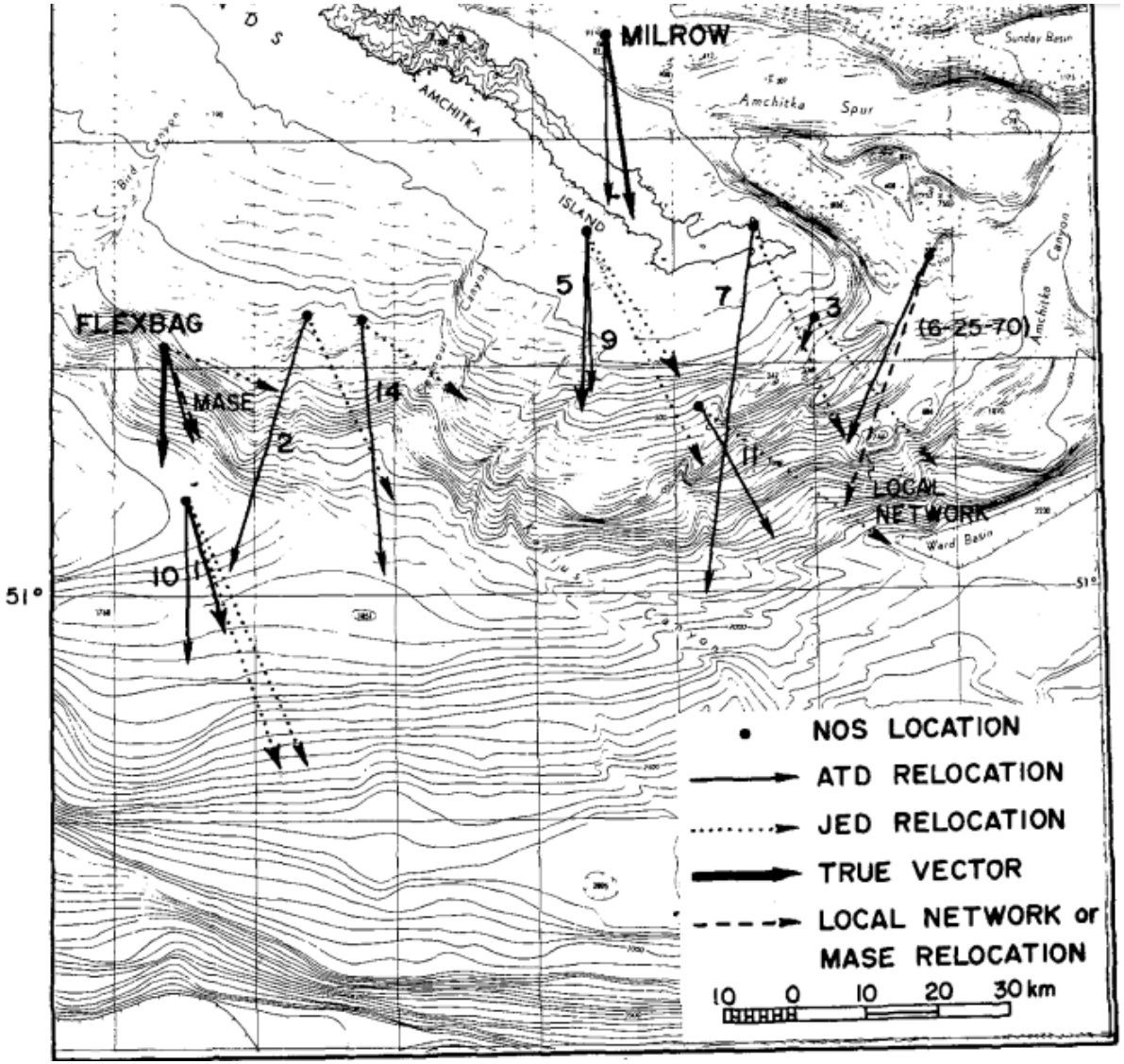
MILROW
FLEXBAG
MASE
LOCAL NETWORK
(6-25-70)
AMCHITKA
ISLAND
Amchitka Spur
Sunday Basin
Ward Basin
Bird Canyon
Amchitka Canyon
51°
NOS LOCATION
ATD RELOCATION
JED RELOCATION
TRUE VECTOR
LOCAL NETWORK or MASE RELOCATION
10 0 10 20 30 km

Double Difference

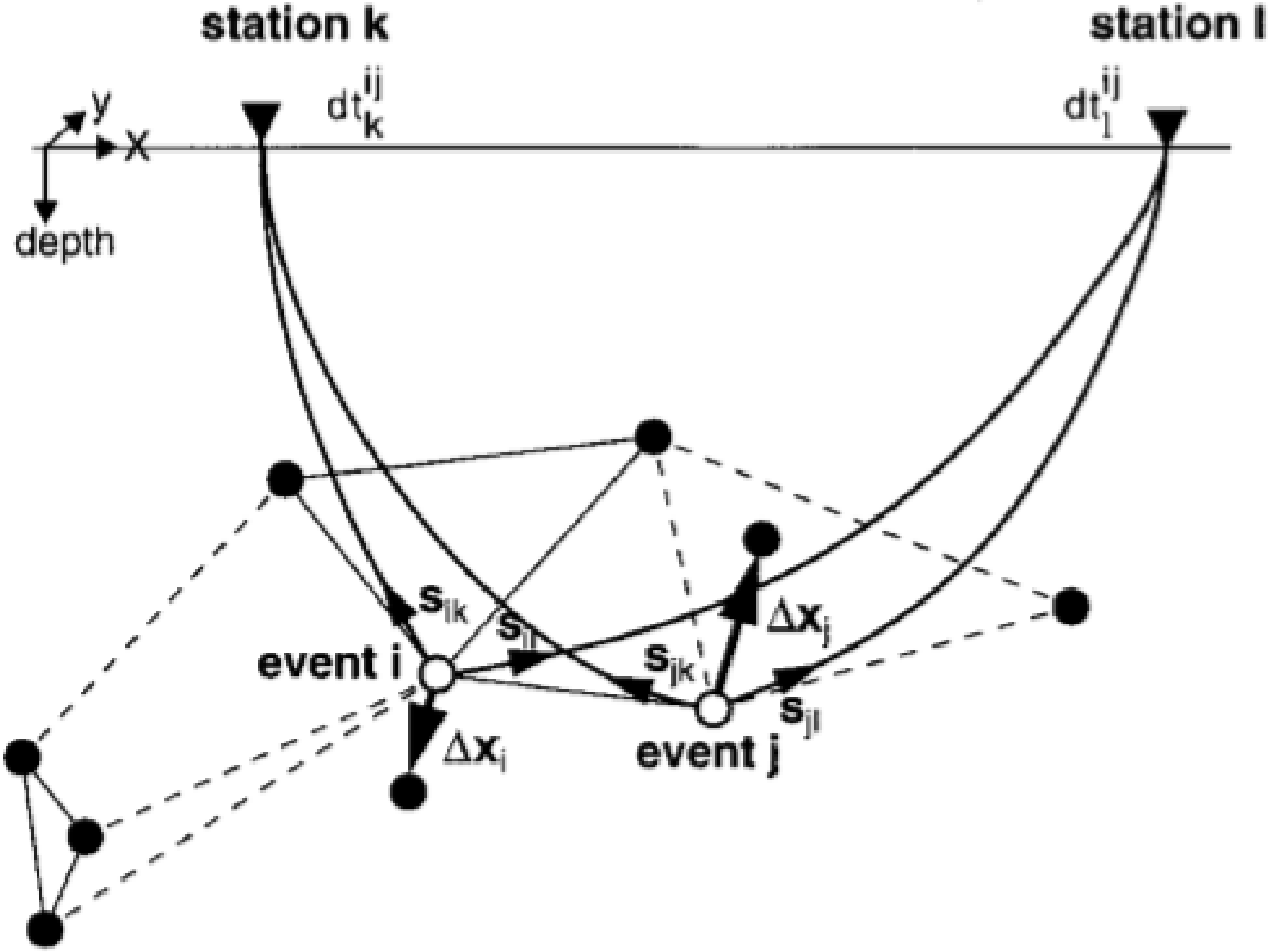

Double Difference

Double Difference

$$dr_k^{ij} = (t_k^i - t_k^j)^{obs} - (t_k^i - t_k^j)^{cal}.$$

$$\frac{\partial t_k^i}{\partial x}\Delta x^i + \frac{\partial t_k^i}{\partial y}\Delta y^i + \frac{\partial t_k^i}{\partial z}\Delta z^i + \Delta\tau^i - \frac{\partial t_k^j}{\partial x}\Delta x^j - \frac{\partial t_k^j}{\partial y}\Delta y^j - \frac{\partial t_k^j}{\partial z}\Delta z^j - \Delta\tau^j = dr_k^{ij}. \quad (6)$$

Reference : Waldhauser, F., Ellsworth, W. L. (2000). A double-difference earthquake location algorithm: Method and application to the northern Hayward fault, California. Bulletin of the Seismological Society of America, 90(6), 1353-1368.

Double Difference Tomography

Table 1

The Absolute Differences between the True Locations and Those from the DD Location Method based on 1D Velocity Model, the DD Location Method based on 3D True Velocity Model, Standard Tomography, and DD Tomography

	Median Value (km)			Standard Deviation (km)		
	Latitude	Longitude	Depth	Latitude	Longitude	Depth
DD location (1D)	1.131	1.235	1.123	0.976	0.941	1.658
DD location (3D)	0.432	0.371	0.296	0.336	0.332	0.479
Standard tomography	0.320	0.295	0.460	0.399	0.342	0.575
DD tomography	0.238	0.218	0.329	0.288	0.314	0.427

Reference : Zhang, H., Thurber, C. H. (2003). Double-difference tomography: The method and its application to the Hayward fault, California. Bulletin of the Seismological Society of America, 93(5), 1875-1889.

Double Difference Tomography

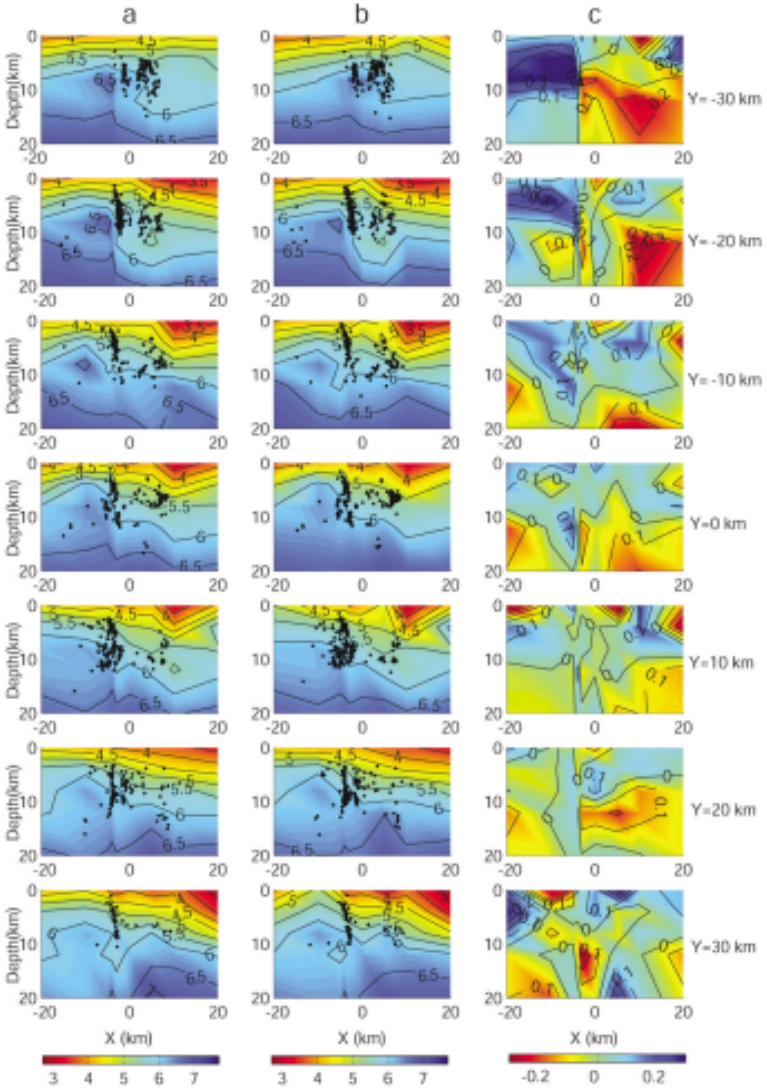

Figure 10. Across-strike vertical slices through (a) the 3D model from DD tomography, (b) the 3D model from standard tomography, (c) the velocity difference between (a) and (b). The final hypocenters within 5 km of each slice are included as black dots.

Thank you!